Evaluation of Surface Melt on the Greenland Ice Sheet Using SMAP *L*-Band Microwave Radiometry

Mohammad Mousavi, *Member, IEEE*, Andreas Colliander, *Senior Member, IEEE*, Julie Z. Miller, Dara Entekhabi, *Fellow, IEEE*, Joel T. Johnson, *Fellow, IEEE*, Christopher A. Shuman, John S. Kimball, *Senior Member, IEEE*, and Zoe R. Courville

***Abstract*—Monitoring melt extent and timing on the Greenland ice sheet is important for tracking the ice sheet's mass and energy balance as well as the global and Arctic climate variability and change. In this study, we use *L*-band (1.4 GHz) brightness temperature observations collected by NASA's soil moisture active passive (SMAP) mission to investigate the extent, duration, and intensity of melt events on the Greenland ice sheet from 2015 to 2021. SMAP provides nearly all-weather surface monitoring over all of Greenland twice daily with morning and evening overpasses at approximately 40-km spatial resolution. We applied empirical threshold and geophysical-model-based algorithms using horizontally and vertically polarized microwave brightness temperature differences to quantify both the intensity and extent of surface melting. Analysis of the melt seasons shows that Greenland experienced unusually strong melt events at the end of July 2019 and on August 14, 2021, which extended the melt area across much of the dry snow zone over a period of one and two days, respectively. *In situ* temperatures measured at Greenland's Summit station confirm the above freezing temperatures during these extreme events.**

***Index Terms*—Earth, electromagnetic propagation, electromagnetic scattering, geophysical inverse problems, ice, microwave radiometry, modeling, multilayered media, satellites, water resources.**

Manuscript received May 28, 2021; revised August 31, 2021; accepted October 14, 2021. Date of publication November 2, 2021; date of current version November 19, 2021. This work was supported in part by the NASA MEaSUREs under Grant 80NSSC18K0980, and in part by Cryospheric Science Program under Grant 80NSSC18K1055. *(Corresponding author: Mohammad Mousavi.)*

Mohammad Mousavi and Andreas Colliander are with the Jet Propulsion Laboratory, California Institute of Technology, Pasadena, CA 91125 USA (e-mail: mousavi@jpl.nasa.gov; andreas.colliander@jpl.nasa.gov).

Julie Z. Miller is with the Cooperative Institute for Research in Environmental Sciences, University of Colorado Boulder, Boulder, CO 80309 USA (e-mail: jzmiller.research@gmail.com).

Dara Entekhabi is with the Massachusetts Institute of Technology, Cambridge, MA 02139 USA (e-mail: darae@mit.edu).

Joel T. Johnson is with the The Ohio State University, Columbus, OH 43210 USA (e-mail: johnson.1374@osu.edu).

Christopher A. Shuman is with the University of Maryland, Baltimore County, Baltimore, MD 21250 USA, and also with the NASA's Goddard Space Flight Center, Greenbelt, MD 20771 USA (e-mail: christopher.a.shuman@nasa.gov).

John S. Kimball is with the Numerical Terradynamic Simulation Group, University of Montana, Missoula, MT 59812 USA (e-mail: john.kimball@mso.umt.edu).

Zoe R. Courville is with the Cold Regions Research and Engineering Laboratory, USACE, Hanover, NH 03755 USA (e-mail: zoe.r.courville@usace.army.mil).

Digital Object Identifier 10.1109/JSTARS.2021.3124229

I. Introduction

ABOUT 8% of the world's ice is located on the Greenland (GL) ice sheet. The melting of this large ice mass over land due to global warming is estimated to contribute approximately 0.72 mm/yr to global sea-level rise [1]–[3]. Due to their all-weather operational capability and sensitivity to the presence of liquid water in snow, both satellite microwave radar and radiometer systems are commonly used to detect melt events over GL [4]–[7].

L-band (1.4 GHz) radiometer systems may provide more comprehensive information on the polar ice sheets because of the larger characteristic ice penetration and sensing depth at lower microwave frequencies, which can extend up to hundreds of meters beneath the surface as compared to higher frequencies [8]–[10]. In this article, we investigated the response of the *L*-band radiometer on NASA's soil moisture active passive (SMAP) satellite, launched in January 2015, to the GL ice sheet's melt events [11]. The objective of this study is to detect dielectric changes in the surface composition, such as snow wetness percentage, and relate those changes to melt events. Our hypothesis is that the long-wavelength (1.4 GHz) measurements from SMAP are more sensitive to a higher melt intensity and deeper surface snow/firn/ice layers than the shorter wavelength measurements used by more conventional satellite microwave radiometers. We use a recently developed algorithm [12] to determine spatial and temporal variations in surface wetness over the GL ice sheet using SMAP brightness temperature (TB) retrievals. Similarly, Houtz *et al.* [13] quantified surface melt on the GL ice sheet using microwave TB measured at 1.4 GHz by the European Space Agency soil moisture and ocean salinity (SMOS) radiometer from 2011 to 2018. They used the microwave emission model of layered snowpacks (MEMLS) [14] with a different layer configuration from our model. The similarities and differences during the overlapped period of investigation (2015–2018) between the results obtained with the model used here [13] are discussed in different sections of this article.

The rest of this article is organized as follows. In Section II, we present the SMAP data and our method to detect melt events using SMAP microwave observations. In Section III, we demonstrate the melt detection and snow wetness retrieval results from both the empirical and the model-based algorithms. Finally, Section IV concludes this article.

II. Data and Methods

A. SMAP Data

NASA launched the SMAP mission on January 31, 2015, and science data production began on March 31, 2015. The *L*-band radiometer onboard the satellite includes vertically (V) and horizontally (H) polarized TB channels. The SMAP TB measurements have a 38-km spatial footprint (defined by the half-power footprint on the earth's surface of the radiometer antenna pattern), and the data are mapped to a 9-km polar equal-area projection grid [15]. The SMAP satellite has a sun-synchronous 6 A.M./6 P.M. equator-crossing orbit, a constant 40° sensor incidence angle, and an approximate 1000-km swath width [16]. This enables daily coverage of the GL ice sheet with both A.M. and P.M. overpasses. The radiometric resolution of the gridded SMAP TB product is less than 0.5 K [16].

B. Method

Due to the strong sensitivity of the microwave TB measurements to the presence of liquid water in snowpack [17], melt detection can be achieved by monitoring the changes of the normalized polarization ratio (NPR) and V-polarized TB with respect to reference values computed during winter conditions, and subsequently, estimating snow wetness for melt events [12]. The NPR is computed as [12]

$$\mathrm{NPR} = \frac{T_{B_v} - T_{B_h}}{T_{B_v} + T_{B_h}} \tag{1}$$

where T_{B_v} and T_{B_h} are the V- and H-polarized TB, respectively. The advantage of using the NPR compared to brightness-based approaches is that it minimizes the sensitivity to the physical temperature [18], [19]. Even though there are some residual differences in the effect of physical temperature on the V- and H-polarized TB, the influence is dominated by the dielectric changes of the wet snow active layer. The benefit of using TBV is to reduce any false melt event detection by the NPR, as the V-pol TB changes are dominated by changes in the dielectric constant, whereas the H-pol TB is affected comparatively by the changes in a vertical layer structure. This can affect the NPR even in the absence of any liquid water.

Fig. 1(a) and (b) shows the regional pattern of the NPR reference value ($\mathrm{NPR}_{\mathrm{ref}}$) and the maximum NPR seasonal difference from reference conditions for the 2016 melt season (MS) (April 7–September 30, 2016), respectively. $\mathrm{NPR}_{\mathrm{ref}}$ is the temporal mean of the NPR from April 1–6 in each calendar year. This one-week duration for the winter reference period is due to the availability of SMAP data starting only in April 2015. Based on the analysis of the length of the winter reference period in [12], this one-week period would be adequate based on our selected Z parameters in (2) and (3) ($Z_{\mathrm{npr}} = 5$ and $Z_{tbv} = 10$). The analysis shows that the NPR value can either increase or decrease from the winter season average depending on the location. A positive NPR change is expected for dry snow conditions or areas that typically experience limited seasonal melting, whereas a negative NPR change is expected for areas with complex subsurface structures that result due to seasonal melting. These scenarios are explained in more detail in [12].

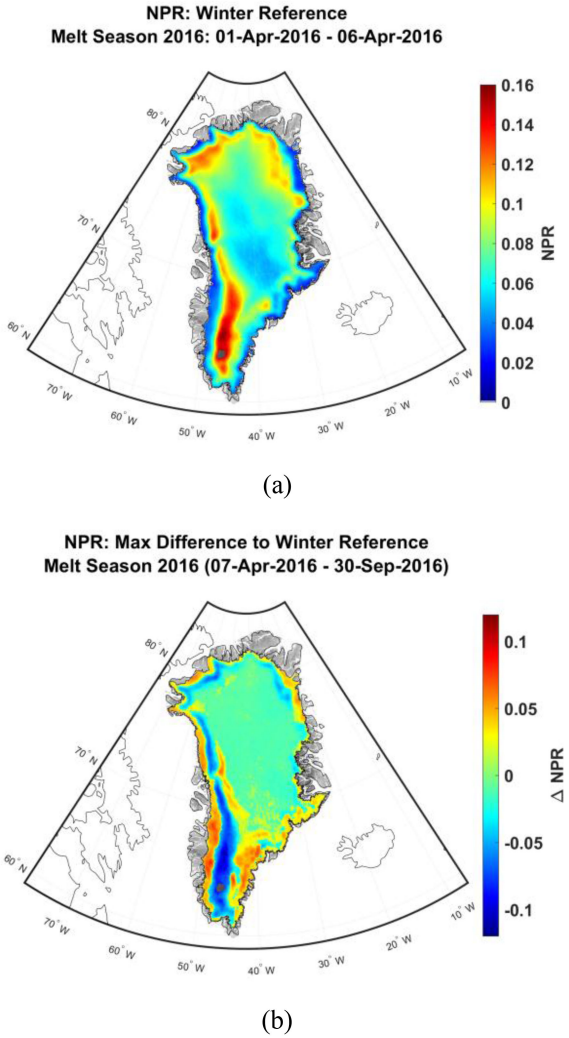

Fig. 1. (a) Maximum of the SMAP $\Delta\mathrm{NPR}$. (b) $\mathrm{NPR}_{\mathrm{ref}}$ for an austral MS (April 7–September 30, 2016) over GL.

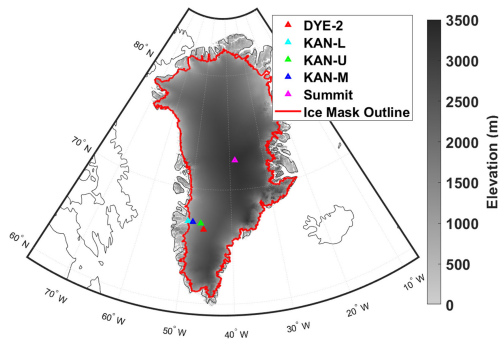

Fig. 2. GL digital elevation map (DEM) with select weather stations shown with symbols.

After monitoring the NPR and T_{B_v} variations, we determine spatial and temporal variations in surface wetness over the GL ice sheet using an empirical threshold algorithm and retrieve snow wetness based on a geophysical multilayer snow

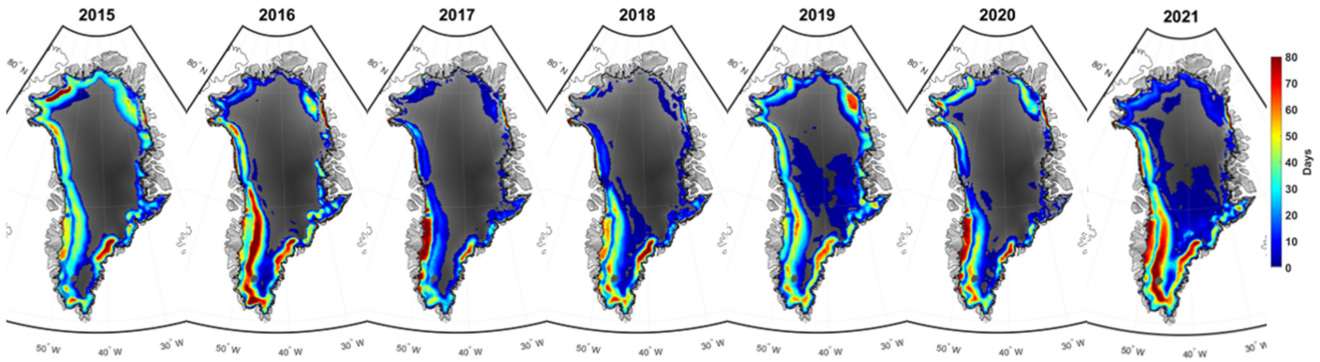

Fig. 3. Number of melt days derived from the empirical algorithm using SMAP *L*-band (1.4 GHz) radiometer TB retrievals over GL for each MS from 2015 to 2021.

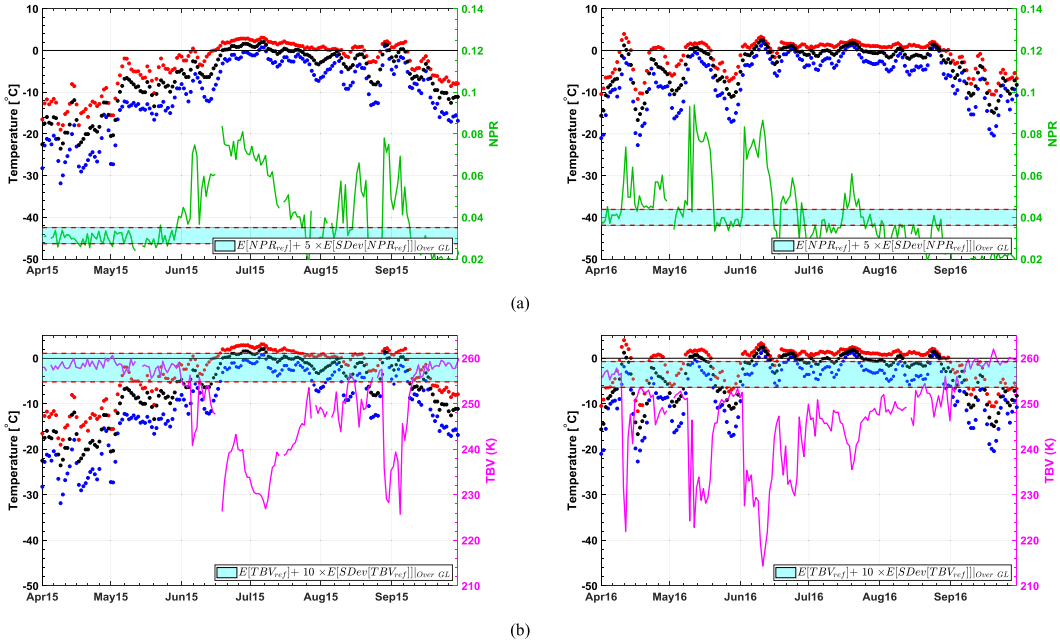

Fig. 4. SMAP measured (a) NPR and (b) V-pol TB over the GL KAN-M station (67.06° N and 48.83° W) during the 2015 and 2016 MSs (April 7–September 30) of the study period. The temperature is measured at the KAN-M station (https://www.promice.dk/WeatherStations.html). Daily maximum, minimum, and average air temperatures are denoted by red, blue, and black dots, respectively. The cyan-shaded regions demonstrate the threshold region above which a melt event would be detected.

emission model and wetness retrieval (SnoWR) algorithm. Both algorithms are explained in more detail in [12]. The algorithms determine that a melt event has occurred if both $\Delta\mathrm{NPR}$ $(=\ \mathrm{NPR}_{\mathrm{daily}} - \mathrm{NPR}_{\mathrm{ref}})$ and ΔT_{BV} $(= T_{BV\,\mathrm{daily}}\ - T_{BV\,\mathrm{ref}})$ are greater than empirically determined threshold values

$$m_1\ (t) = \begin{cases} 1\ (\mathrm{True}) & |\Delta\mathrm{NPR}| \geq Z_{\mathrm{npr}} \times E[SD\,[\mathrm{NPR}]\,|_{W\mathrm{REF}}]_{\mathrm{All\ Pixels}} \\ 0\ (\mathrm{False}) & \mathrm{otherwise} \end{cases} \tag{2}$$

$$m_2\ (t) = \begin{cases} 1\ (\mathrm{True}) & |\Delta\mathrm{T_{BV}}| \geq Z_{tbv} \times E[SD\,[T_{BV}]\,|_{W\mathrm{REF}}]_{\mathrm{All\ Pixels}} \\ 0\ (\mathrm{False}) & \mathrm{otherwise} \end{cases} \tag{3}$$

where E[] is the mean estimator, SD[] is the temporal standard deviation (STD) estimator, WREF refers to the time period from April 1–6, All Pixels refers to taking the spatial average over all GL pixels, and Z_{npr} and Z_{tbv} are constant real numbers. The Z parameter determines the false alarm rate [12], [20]. A melt event will be detected at time t if both $m_1(t)$ and $m_2(t)$ indicate melt occurrence, which corresponds to a bitwise AND operation Λ on the $m_1(t)$ and $m_2(t)$ binary states.

After detecting a melt event, the snow wetness is retrieved using the SnoWR algorithm [12]. The algorithm uses microwave emission models for either decrease or increase scenarios of the NPR during MSs. The emission model represents a three-layer medium (air, wet snow, and dry snow layers) for the case of increasing NPR, and a four-layer medium for the case of decreasing NPR by adding a middle layer between the wet and dry snow layers of the three-layer model. Four different look-up tables (LUTs) describing the vertical and horizontal TB response

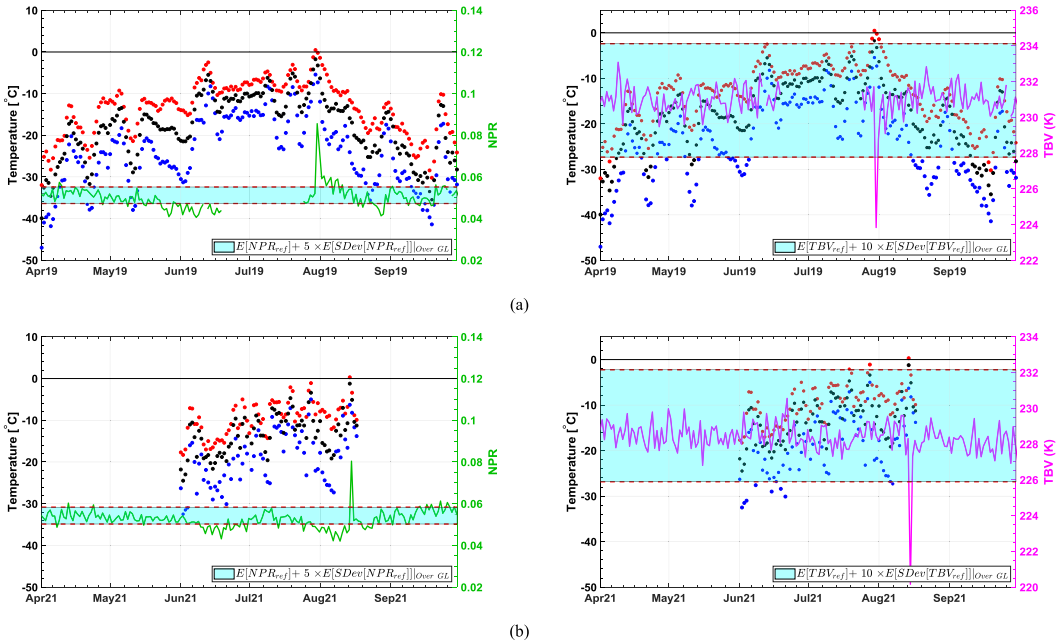

Fig. 5. SMAP measured (left) NPR and (right) V-pol TB over the GL Summit weather station (72.58° N and 38.46°) during the (a) 2019 and (b) 2021 MSs (April 7–September 30) of the study period. The temperature is measured at the Summit station (https://www.esrl.noaa.gov/gmd/obop/sum/). Daily maximum, minimum, and average air temperatures are denoted by red, blue, and black dots, respectively. The cyan-shaded regions demonstrate the threshold region above which a melt event would be detected.

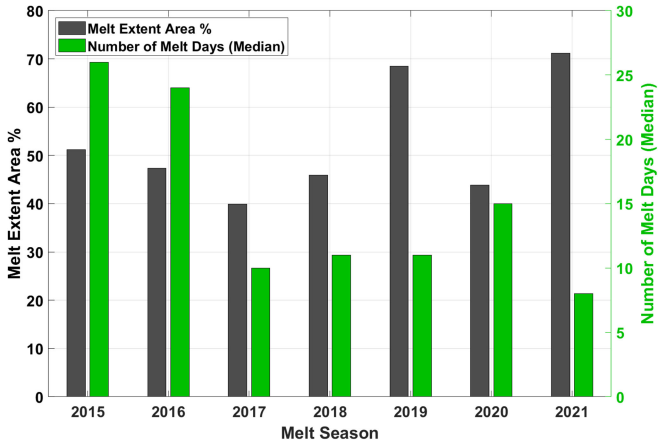

Fig. 6. Total melt area percentage and the median number of melt days derived from the empirical threshold algorithm over GL for seven MSs between 2015 and 2021.

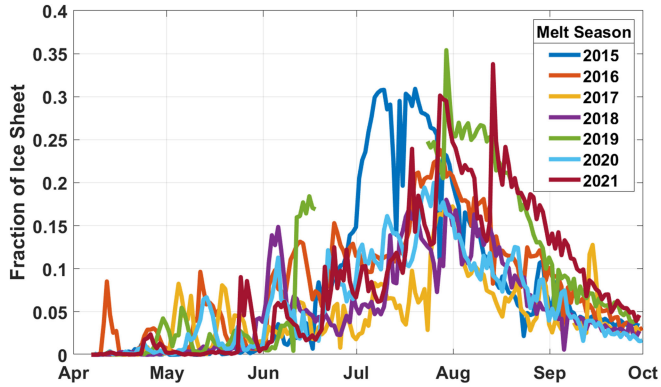

Fig. 7. Daily melt area of GL derived from the empirical algorithm using SMAP *L*-band microwave radiometry between 2015 and 2021. The MSs are color coded.

during melt and freeze seasons (FSs) were made by sweeping the model parameters over specified realistic ranges. The top wet snow layer is absent in the models during the frozen season. Finally, layer properties, such as snow wetness and density, are retrieved by comparing the SMAP measured TB with the LUTs during melt and FSs.

In contrast, Houtz *et al.* [13] used a four-layer model configuration (air, wet snow, dry snow, and ice substrate) of MEMLS over all of GL. This difference in the snow model configurations does not mean that either of the approaches is superior to the other. Indeed, it suggests that there is no single optimal model configuration for the entire GL ice sheet due to its large area and the spatial variability of snow physical properties. Hence, by selecting an appropriate snow model, an algorithm can be developed, similar to this article and [13], to retrieve the desired snow parameters, such as wetness and density.

III. Results

A. Empirical Algorithm Results

Fig. 2 shows the GL DEM with various weather stations denoted in [21]. The GL ice mask, based on the Programme for Monitoring of the GL Ice Sheet (PROMICE), used in this study is derived from the analysis of an aerophotogrammetric map of GL acquired in the 1980s [22]. The purpose of using the ice mask is to ensure that the SMAP footprint is only over the ice sheet and not bare ground, as the seasonal behavior of TB would be different. However, due to the coarse resolution

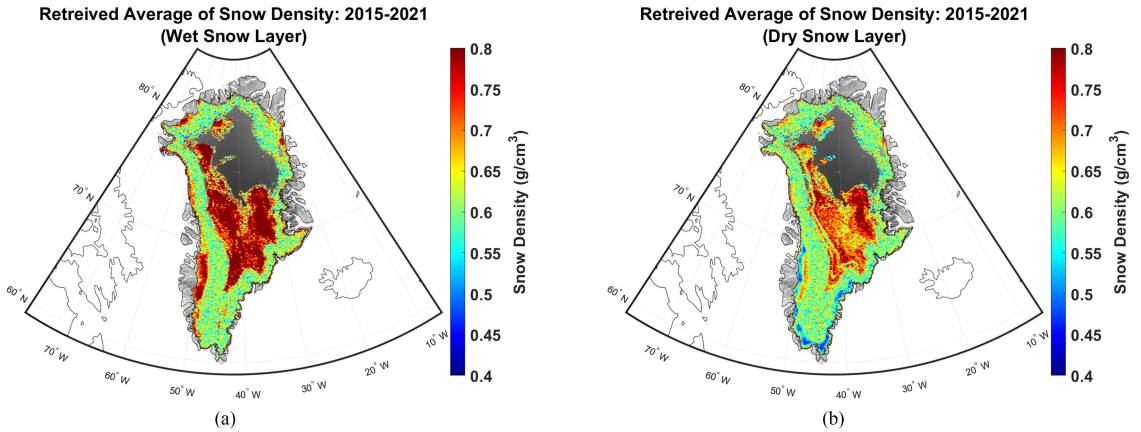

Fig. 8. Retrieved temporal mean snow density using the SnoWR algorithm from 2015 to 2021 during (a) melt and (b) frozen seasons overlaid on the gray shaded DEM.

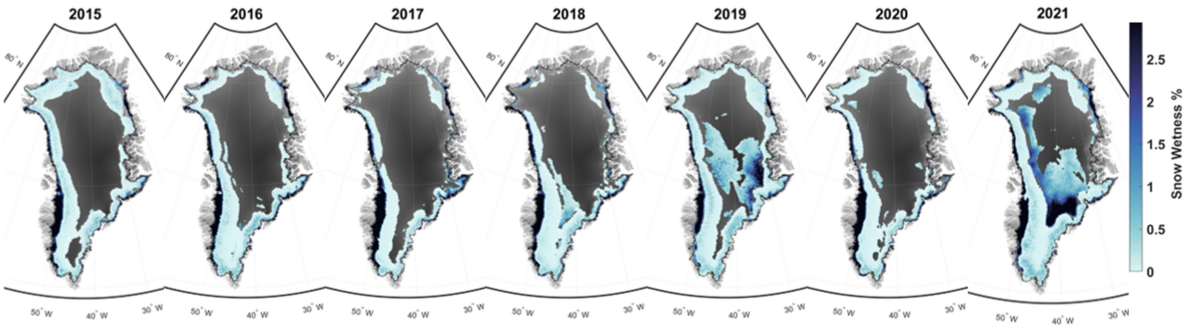

Fig. 9. SMAP retrieved temporal mean snow wetness percentage using the SnoWR algorithm over GL for each MS from 2015 to 2021, overlaid on the gray shaded DEM.

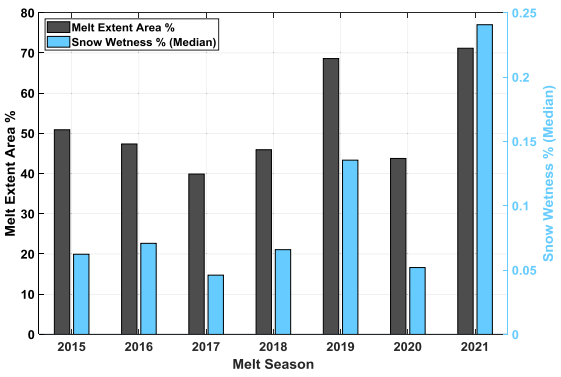

Fig. 10. Bar chart for the total melt area percentage and the median of the snow wetness percentage over GL retrieved from SMAP TB observations using the SnoWR algorithm.

SMAP gridding and the ice mask imperfections, there may still be mixing of the ice sheet and bare ground emissions along the ice mask edges. This ice mask outline is shown with a red solid line in Fig. 2. In this study, the MS and the winter reference periods are April 7–September 30 and April 1–6 in each calendar year, respectively. The potential MSs start after the last day of their winter reference period.

Fig. 3 shows the melt detection results for each MS using the empirical melt detection algorithm [12] overlaid on the GL DEM. There is very little interannual variability in the $\mathrm{NPR}_{\mathrm{ref}}$ and $T_{BV_{\mathrm{ref}}}$ values (see Figs. 13 and 14 in Appendix A; the figures also show $\Delta\mathrm{NPR}$ and ΔT_{BV} for each MS). Fig. 15 shows the STD of $\mathrm{NPR}_{\mathrm{ref}}$ and $T_{BV_{\mathrm{ref}}}$ from 2015 to 2021. The maximum values are 0.0147 and 13.33 K for $\mathrm{NPR}_{\mathrm{ref}}$ and $T_{BV_{\mathrm{ref}}}$, respectively, and their corresponding mean values are 0.003 and 1.514 K. The southwest coast of the GL ice sheet experienced melt events in all of the MSs covered by the SMAP record and has the largest number of melt days during 2016, 2017, 2020, and 2021 MSs, as shown in Fig. 3. As an example, Fig. 4(a) and (b) shows NPR and T_{BV}, respectively, measured by SMAP over the KAN-M weather station (67.06° N and 48.83° W) during the 2015 and 2016 MSs. This station is located at an elevation of 1500 m above sea level (a.s.l). The air temperature data for this station from the PROMICE website[1] shows that there was a greater number of melt days (indicated by measured air temperatures above 0.0 °C) in 2016 than in 2015. Other KAN stations (KAN-L and KAN-U) show similar behavior (only KAN-M results are shown for brevity). Therefore, the station

[1][Online]. Available: https://www.promice.dk/WeatherStations.html

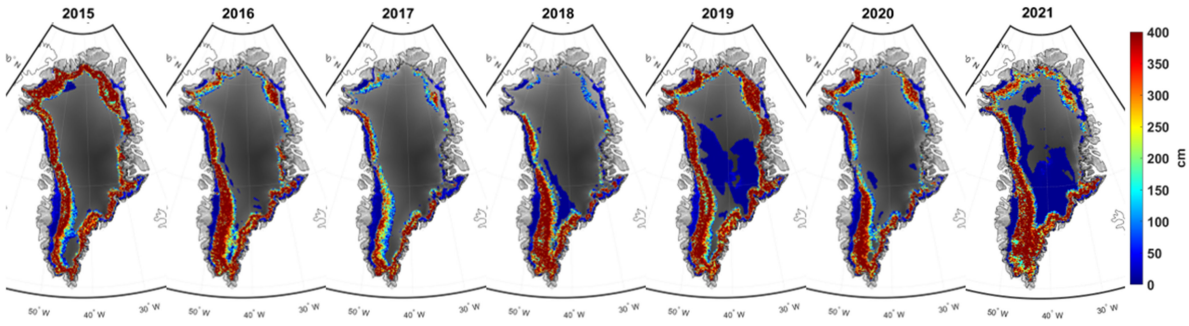

Fig. 11. Retrieved wet snow layer thickness using the SnoWR algorithm over GL for each MS from 2015 to 2021.

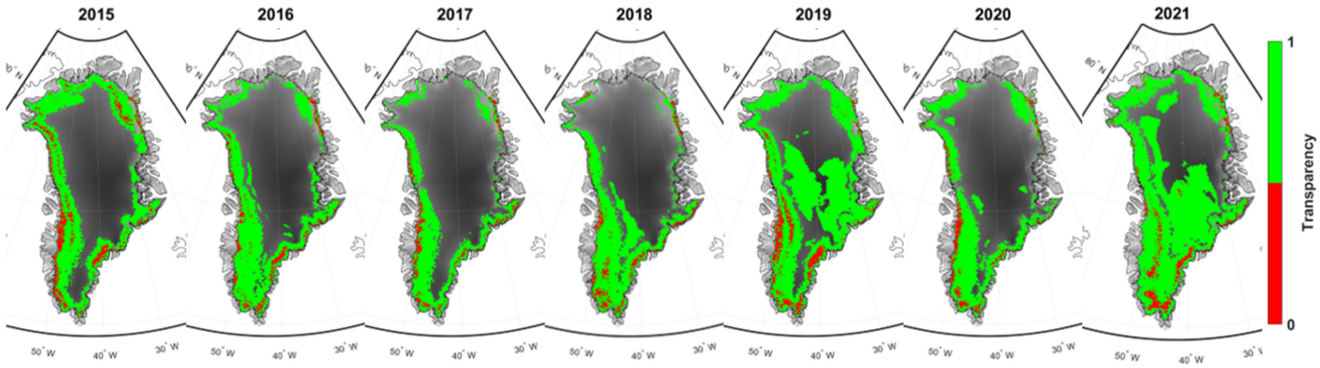

Fig. 12. Top wet snow layer binary transparency state, 1 (green) as transparent and 0 (red) as opaque, using the SnoWR algorithm over GL for each MS from 2015 to 2021. The transparency state is calculated using the maximum snow wetness during each MS.

measurements support the result retrieved with the empirical algorithm.

The maps show that the interior of the GL ice sheet experienced melt events only during MSs 2019 and 2021 for less than 10 days. The closest weather station to this part of GL is the Summit station (72.58° N and 38.46° W). Fig. 5(a) and (b) shows the NPR and T_{BV} observations over Summit station during the 2019 and 2021 MS (April 7–September 30), respectively. This station is located at an elevation of 3200 m a.s.l. The figures also show *in situ* air temperature measurements from Summit station acquired from the National Oceanic and Atmospheric Administration, Earth System Research Laboratory, Global Monitoring Division.[2] On July 31, 2019 and August 14, 2021, the air temperature rose above the water freezing point (0 °C), and there was a significant change in the measured NPR (increase) and T_{BV} (decrease), with both falling outside their corresponding thresholds (cyan shaded region) indicating melt detection. This melt event happened over about one day, which agrees with the number of melt days for this location in Fig. 3.

The region to the east of the melt area over the high-elevation GL interior (∼ 73.00° N and 31.00° W) experienced more melt events during the 2019 MS. The northern part of GL along the coast also experienced more melt events during 2015, 2019, 2020, and 2021, with the 2019 and 2021 MSs having the greatest number of melt days and extent along the northern coastal region. In general, the 2019 and 2021 MSs experienced the largest melt extents (∼69%) as a result of the exceptional melt event at the end of July 2019 and on August 14, 2021 over the GL interior. A similar melt extent area of about 62% of GL during 2019 is reported in [23].

[2][Online]. Available: https://www.esrl.noaa.gov/gmd/obop/sum/

TABLE I
TOTAL MELT AREA PERCENTAGE AND THE MEDIAN NUMBER OF MELT DAYS DERIVED FROM SMAP *L*-BAND TB RETRIEVALS USING THE EMPIRICAL ALGORITHM AND THE MEDIAN OF THE SNOW WETNESS PERCENTAGE RETRIEVED USING THE SNOWR ALGORITHM OVER GL

Melt Season	Total Melt Area %	Median of the Number of Melt Days	Median of the Retrieved Snow Wetness %
2015	50.89 %	25	0.06 %
2016	47.36 %	24	0.07 %
2017	39.88 %	10	0.04 %
2018	45.93 %	11	0.07 %
2019	68.60 %	10	0.14 %
2020	43.76 %	15	0.05 %
2021	71.17 %	8	0.24 %

Columns 2 and 3 of Table I show the melt area percentage (ratio of the number of melt pixels by the total number of pixels over GL and within the ice sheet mask) and median of the number of melt days derived from the empirical algorithm over GL in each annual MS, respectively. Fig. 6 illustrates the results in columns 2 and 3 of Table I in a bar chart format. The melt maps show the melt extent and duration across GL, but they do not convey the intensity of the melt, which we derived using the snow wetness retrieval and discussed in the next section. The median number of melt days is highest during the 2015 MS.

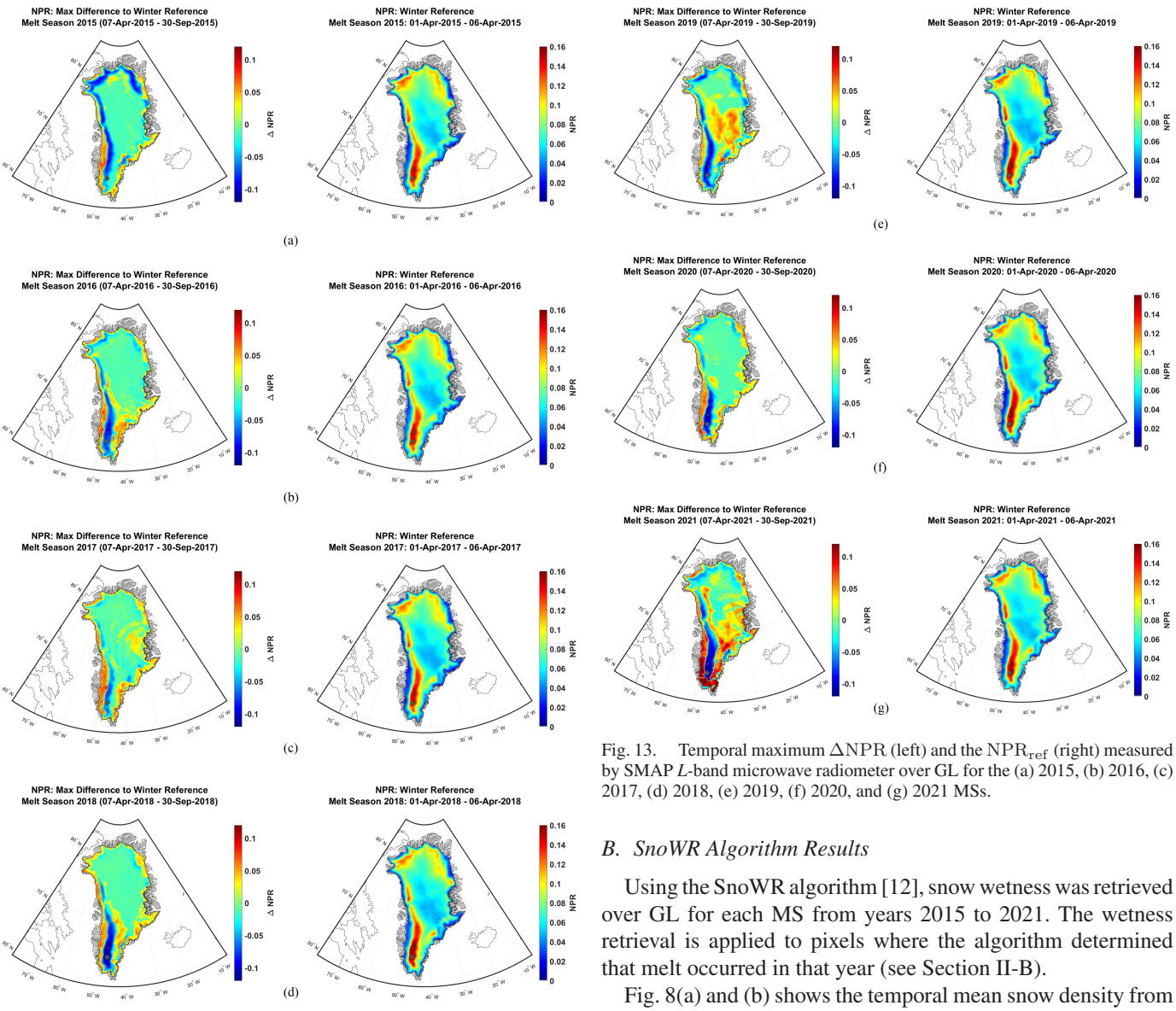

Fig. 13. Temporal maximum $\Delta\mathrm{NPR}$ (left) and the $\mathrm{NPR_{ref}}$ (right) measured by SMAP *L*-band microwave radiometer over GL for the (a) 2015, (b) 2016, (c) 2017, (d) 2018, (e) 2019, (f) 2020, and (g) 2021 MSs.

Even though 2015 did not experience the largest number of melt days along the southwest coast, it experienced a more uniform number of melt days along most of the GL coastal region, which resulted in 2015 having the largest median number of melt days. Moreover, the median number of melt days was particularly low in 2017, 2018, 2019, and 2021, whereas the largest melt extent area occurred in 2019 and 2021.

Fig. 7 shows the evolution of the melt extent over GL (daily ratio of the cumulative number of melt pixels by the total number of pixels over the GL ice sheet) from April 1 to September 30 of each calendar year. While the timing of the maximum melt and the overall duration of the MS is fairly consistent from year to year, the results show that 2019 and 2021 have a large and narrow spike in melt extent at the end of July and on August 14, respectively, which corresponds to brief periods of anomalous surface melting (less than 10 days) that occurred over the high-elevation GL interior. The curves also clearly show the next largest melt extent of the 2015 MS.

B. SnoWR Algorithm Results

Using the SnoWR algorithm [12], snow wetness was retrieved over GL for each MS from years 2015 to 2021. The wetness retrieval is applied to pixels where the algorithm determined that melt occurred in that year (see Section II-B).

Fig. 8(a) and (b) shows the temporal mean snow density from 2015 to 2021 during the respective MS and FS. The plots are overlaid on the GL DEM. The spatial mean of the retrieved snow densities during the MS and FS are about 683 and 641 $\mathrm{kg/m^3}$, respectively. As an example, the retrieved average snow density and thickness of the top wet snow layer during the MS 2016 at DYE-2 station ($\sim$66.49° N and 46.30° W) are 493 $\mathrm{kg/m^3}$ and 7.5 m. The reported *in situ* values of the mean snow density over the first 3.7 m of snow at two different snow pits ($\sim$400 m apart) at the DYE-2 station from May to September 2016 are 406 ± 93.5 and 436 ± 153.2 $\mathrm{kg/m^3}$, respectively [24]. Houtz *et al.* [13] reported a mean retrieved snow density of about $600\pm50\,\mathrm{kg/m^3}$ from 2011 to 2018. The correspondence is reasonable considering the large snow density variability within and between the snow pits, and the fact that the retrieval is attributing the density to deeper (generally denser) layers not captured by the snow pit measurements.

Fig. 9 shows the temporal mean snow wetness percentage retrieved across GL. The figure shows that the GL ice sheet experienced more wetness along the southwest coastal region in all MSs. Similar results showing more wetness along the coastal

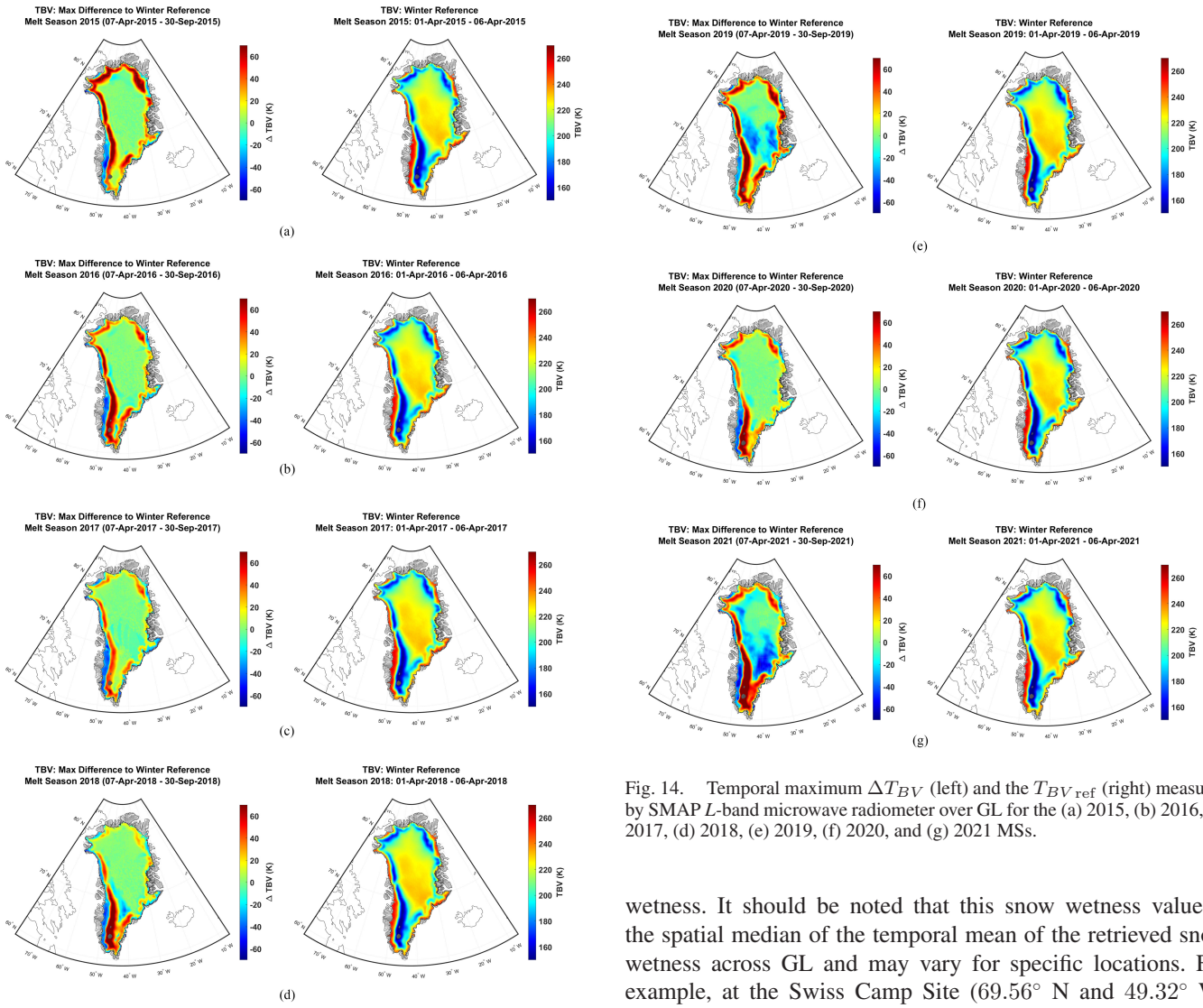

Fig. 14. Temporal maximum ΔT_{BV} (left) and the $T_{BV\,\mathrm{ref}}$ (right) measured by SMAP L-band microwave radiometer over GL for the (a) 2015, (b) 2016, (c) 2017, (d) 2018, (e) 2019, (f) 2020, and (g) 2021 MSs.

regions (especially in the southern region) are shown in [13] from 2015 to 2018, as they only retrieved wetness from 2011 to 2018. Colosio *et al.* [25] used higher frequency (37 GHz) measurements of SMMR and SSMI/S, also reported melt events along the coastal regions with an increasing number of melt days mostly in western GL. However, in 2019, a smaller area near the southwest coast experienced a higher snow wetness percentage compared to the other MSs. GL also experienced more wet snow to the east of the GL interior during the July 2019 melt event. In addition, in 2021, the interior area along the northwest coast experienced more wetness compared to the other MSs. These results agree with the map of the number of melt days from the empirical algorithm in Fig. 3.

Column 4 of Table I represents the median of the snow wetness percentage over GL, retrieved using the SnoWR algorithm in each MS. Fig. 10 illustrates the results in columns 2 and 4 of Table I in a bar chart format. The 2019 and 2021 MSs had the most extensive melting with the top two median snow wetness percentages of 0.14% and 0.24%, respectively, over GL. Even though GL did not experience a longer period of melting in 2019 and 2021, as shown in Fig. 6, it experienced greater snow wetness. It should be noted that this snow wetness value is the spatial median of the temporal mean of the retrieved snow wetness across GL and may vary for specific locations. For example, at the Swiss Camp Site (69.56° N and 49.32° W) during 2015, the temporal maximum retrieved snow wetness and the retrieved wet snow layer thickness are about 9% and 44 cm, respectively. Other studies, using higher frequency (37 GHz) satellite microwave TB observations, reported a similar temporal liquid water percentage with a maximum value of about 9% and 8% averaged over the first 5 cm and 1 m of snow, respectively, at the Swiss Camp site during 2001 [25].

The wet snow layer thickness depends on the depth of the near-surface layer warming and the percolation of melt water from the warm top layers into the deeper otherwise dry snow layers. Longer melt periods promote the percolation of melt water into deeper firn layers. The successful detection of the wet layer thickness depends on the magnitude of the wetness, as a very wet surface would hinder emissions from the deeper layers, and the retrieved wet layer thickness could appear thinner than it actually is. However, as melt water percolates downward the volumetric snow wetness may remain low enough for L-band penetration even for longer melt periods. For example, using Figs. 9 and 11, the retrieved wet snow layer was relatively thick (∼700 cm) over the region to the east of the southwest Gl coastline (∼68.00° N and 49.00° W) during 2019, where the melt event was less intense (temporal mean snow wetness ∼ 0.2%), and the microwave signal could penetrate deeper into

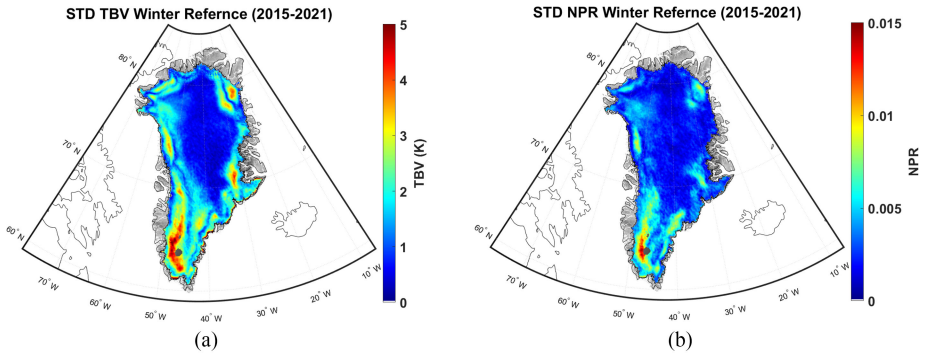

Fig. 15. STDs of $T_{BV\,\mathrm{ref}}$ (left) and $\mathrm{NPR}_{\mathrm{ref}}$ (right) measured by SMAP *L*-band microwave radiometer over GL from 2015 to 2021.

the layer. Conversely, for ice shelves closer to the southwest coastline, the retrieved wet snow layer was relatively thin (<30 cm) during the 2019 MS, as the melt events were more intense (snow wetness $\sim 2.3\%$). However, it should be noted that liquid water percolation in the snow layer is complex and influenced by many factors, such as blockage by ice lenses and retention of liquid water at varying snow layer depths [24]. Fig. 11 shows the retrieved wet snow layer thickness over GI for each MS from 2015 to 2021.

The wet snow in the surface attenuates microwave emissions from deeper ice layers, which creates uncertainty regarding the true thickness of the wet layer for very wet conditions. The penetration depth for a medium is computed using retrieved snow density and the temporal maximum retrieved snow wetness. If the penetration depth was larger than the wet snow layer thickness (more than 1/e of the radiation passing through the layer), then the layer of the pixel was classified as transparent; if it was smaller, then the pixel was classified as opaque [12]. Based on this classification, most of GL was transparent during melt events, except for regions closer to coastlines, particularly the southwest. For those regions, the wet snow layer thickness remains uncertain and may be thicker than the retrieval would indicate. A smaller part of the southwest coastal region became opaque during 2016 and 2018, compared to other years of record. In addition, the GL interior, which experienced only a brief period (less than 10 days) of melting, is mostly transparent. Fig. 12 shows the binary transparency state of the top wet snow layer over GL for each MS from 2015 to 2021.

IV. Conclusion

This study demonstrates the potential of SMAP *L*-band radiometry for tracking ice sheet melt events over GL. We use a recently developed geophysical model (SnoWR) and empirical algorithms to estimate the duration and intensity of surface melting over GL solely using SMAP *L*-band TB observations. The approach exploits the effect of liquid water in the surface layers of the ice sheet on *L*-band radiation. Unlike higher frequency (shorter wavelength) observations, the SMAP low-frequency (1.41 GHz) observations can sense deeper into the snow/firn layers and slowly saturate with the presence of liquid water even in deep layers of the ice sheet. The results show that most of the lower elevation GL coastal regions experienced melt events during all MSs from 2015 to 2021. The southwest coast also experienced a fairly high number of melt days and snow wetness during all MSs. In addition, GL had exceptionally strong melt events at the end of July 2019 and on August 14, 2021, which extended the melt area across much of the GL high-elevation interior and dry snow zone over an average period of two days. *In situ* air temperatures obtained from GL's Summit station (72.58° S and 38.46° W) indicated above freezing temperatures during these events. Our results also indicated that the 2015 MS had the highest median number of melt days (25 days), whereas the 2021 MS had one of the lowest median number of melt days (6 days) besides the 2019 MS (10 days). This indicates that even though surface melting during 2019 and 2021 happened over most of GL ($\sim$69%) with a larger amount of wetness values (median of 0.14% and 0.20%, respectively, across GL), the 2019 and 2021 melt events happened over a shorter period.

Appendix

See Figs. 13–15.

Acknowledgment

The research described in this publication was carried out at the Jet Propulsion Laboratory, California Institute of Technology, under a contract with the National Aeronautics and Space Administration.

References

[1] W. Krabill *et al.*, "Greenland ice sheet: High-elevation balance and peripheral thinning," *Science*, vol. 289, pp. 428–430, 2000.
[2] E. Rignot, I. Velicogna, M. R. van den Broeke, A. Monaghan, and J. T. M. Lenaerts, "Acceleration of the contribution of the Greenland and Antarctic ice sheets to sea level rise," *Geophys. Res. Lett.*, vol. 38, no. 5, 2011, Art. no. L05503, doi: 10.1029/2011GL046583.
[3] R. Forsberg *et al.*, "Greenland and Antarctica ice sheet mass changes and effects on global sea level," *Surv. Geophys.*, vol. 38, 2017, pp. 89–104, doi: 10.1007/s10712-016-9398-7.
[4] I. S. Ashcraft and D. G. Long, "SeaWinds views Greenland," in *Proc. IEEE Int. Geosci. Remote Sens. Symp. Taking Pulse Planet: Role Remote Sens. Manage. Environ.*, 2020, pp. 1131–1133.
[5] T. L. Mote and M. R. Anderson, "Variations in snowpack melt on the Greenland ice sheet based on passive-microwave measurements," *J. Glaciol.*, vol. 41, no. 137, pp. 51–60, 1995.
[6] T. L. Mote, M. R. Anderson, K. C. Kuivinen, and C. M. Rowe, "Passive microwave-derived spatial and temporal variations of summer melt on the Greenland ice sheet," *Ann. Glaciol.*, vol. 17, pp. 233–238, 1993.
[7] V. Wismann, "Monitoring of seasonal snowmelt on Greenland with ERS scatterometer data," *IEEE Trans. Geosci. Remote Sens.*, vol. 38, no. 4, pp. 1821–1826, Jul. 2000.

[8] K. C. Jezek *et al.*, "500–2000-MHz brightness temperature spectra of the Northwestern Greenland ice sheet," *IEEE Trans. Geosci. Remote Sens.*, vol. 56, no. 3, pp. 1485–1496, Mar. 2018.
[9] J. Z. Miller *et al.*, "Brief communication: Mapping Greenland's perennial firn aquifers using enhanced-resolution L-band brightness temperature image time series," *Cryosphere*, vol. 14, pp. 2809–2817, 2020.
[10] K. C. Jezek *et al.*, "Radiometric approach for estimating relative changes in intraglacier average temperature," *IEEE Trans. Geosci. Remote Sens.*, vol. 53, no. 1, pp. 134–143, Jan. 2015.
[11] D. Entekhabi *et al.*, "The soil moisture active passive (SMAP) mission," *Proc. IEEE*, vol. 98, no. 5, pp. 704–716, May 2010.
[12] M. Mousavi, A. Colliander, J. Z. Miller, and J. Kimball, "A novel approach to map the intensity of surface melting on the Antarctica ice sheet using SMAP L-band microwave radiometry," *IEEE J. Sel. Topics Appl. Earth Observ. Remote Sens.*, 2021.
[13] D. Houtz, C. Mätzler, R. Naderpour, M. Schwank, and K. Steffen, "Quantifying surface melt and liquid water on the Greenland ice sheet using L-band radiometry," *Remote Sens. Environ.*, vol. 256, 2021, Art. no. 112341.
[14] M. Schwank *et al.*, "Model for microwave emission of a snow-covered ground with focus on l band," *Remote Sens. Environ.*, vol. 154, pp. 180–191, 2014.
[15] J. Chaubell, S. Chan, R. S. Dunbar, J. Peng, and S. Yueh, "SMAP enhanced L1C radiometer half-orbit 9 km EASE-grid brightness temperatures, version 1," NASA Nat. Snow Ice Data Center Distributed Active Archive Center, Boulder, CO, USA, 2016.
[16] J. R. Piepmeier *et al.*, "SMAP L-band microwave radiometer: Instrument design and first year on orbit," *IEEE Trans. Geosci. Remote Sens.*, vol. 55, no. 4, pp. 1954–1966, Apr. 2017.
[17] F. Ulaby and D. Long, *Microwave Radar and Radiometric Remote Sensing*. Norwood, MA, USA: Artech House, 2014.
[18] A. Roy *et al.*, "Evaluation of spaceborne L-band radiometer measurements for terrestrial freeze/thaw retrievals in Canada," *IEEE J. Sel. Topics Appl. Earth Observ. Remote Sens.*, vol. 8, no. 9, pp. 4442–4459, Sep. 2015.
[19] K. Rautiainen *et al.*, "Detection of soil freezing from L-band passive microwave observations," *Remote Sens. Environ.*, vol. 147, pp. 206–218, 2014.
[20] S. Mousavi, R. D. De Roo, K. Sarabandi, A. W. England, S. Y. E. Wong, and H. Nejati, "Lake icepack and dry snowpack thickness measurement using wideband autocorrelation radiometry," *IEEE Trans. Geosci. Remote Sens.*, vol. 56, no. 3, pp. 1637–1651, Mar. 2018.
[21] I. M. Howat, A. Negrete, and B. E. Smith, "The Greenland ice mapping project (GIMP) land classification and surface elevation data sets," *Cryosphere*, vol. 8, no. 4, pp. 1509–1518, 2014.
[22] M. Citterio and A. P. Ahlstrom, "Brief communication 'The aerophotogrammetric map of Greenland ice masses'," *Cryosphere*, vol. 7, no. 2, pp. 445–449, 2013.
[23] R. I. Cullather *et al.*, "Anomalous circulation in July 2019 resulting in mass loss on the Greenland ice sheet," *Geophysical Res. Lett.*, vol. 47, no. 17, 2020, Art. no. e2020GL087263.
[24] S. Samimi, S. J. Marshall, and M. MacFerrin, "Meltwater penetration through temperate ice layers in the percolation zone at DYE-2, Greenland ice sheet," *Geophys. Res. Lett.*, vol. 47, no. 15, 2020, Art. no. e2020GL089211.
[25] P. Colosio, M. Tedesco, X. Fettweis, and R. Ranzi, "Surface melting over the Greenland ice sheet from enhanced resolution passive microwave brightness temperatures (1979–2019)," *Cryosphere Discussions*, vol. 15, no. 6, pp. 2623–2646, 2021.

Mohammad Mousavi (Member, IEEE) received the B.S. degree from Shahid Beheshti University, Tehran, Iran, in 2012, and the M.S. and Ph.D. degrees from the University of Michigan, Ann Arbor, MI, USA, in 2015 and 2020, respectively, all in electrical engineering.

His Ph.D. dissertation topic was on developing a microwave radar remote-sensing instrument to measure the thickness of a lake icepack and a dry snowpack. Since 2020, he has been a Postdoctoral Research Fellow with the Jet Propulsion Laboratory, California Institute of Technology, Pasadena, CA, USA. He is also a member of the SMAP science team, where he is working on an active–passive soil moisture retrieval algorithm. His research interests include microwave radar and radiometric remote sensing, electromagnetic scattering, and antennas.

Andreas Colliander (Senior Member, IEEE) received the M.Sc. (Tech.), Lic.Sc. (Tech.), and D.Sc. (Tech.) degrees from Aalto University, Espoo, Finland, in 2002, 2005, and 2007, respectively in all are electrical engineering.

He is currently a Research Scientist with the Jet Propulsion Laboratory, California Institute of Technology, Pasadena, CA, USA. He is also leading the calibration and validation of the geophysical retrievals of NASA's SMAP mission and developing multifrequency retrievals for ice sheets and polar atmosphere. His research interest focuses on the development of microwave remote-sensing techniques.

Julie Z. Miller received the B.S. degree in applied mathematics and the M.S. and Ph.D. degrees in geography, with a focus on microwave remote sensing of ice sheets, from the University of Utah, Salt Lake City, UT, USA, in 2010, 2012, and 2019, respectively.

Then, she completed a postdoctoral fellowship from Byrd Polar and Climate Research Center, The Ohio State University, Columbus, OH, USA. She is currently a Research Scientist with Earth Science and Observation Center, Cooperative Institute for Research in Environmental Sciences, University of Colorado, Boulder, CO, USA. She is also a member of NASA's SMAP Science Team. Her research interest focuses on developing algorithms to map surface and subsurface meltwater in Greenland and Antarctica using multifrequency microwave radiometer and radar scatterometer data.

Dr. Miller has participated in field and airborne campaigns in both Greenland and Antarctica.

Dara Entekhabi (Fellow, IEEE) received the B.S. and M.S. degrees in geography from Clark University, Worcester, MA, USA, in 1983, 1985 and 1987, respectively, and the Ph.D. degree in civil and environmental engineering from the Massachusetts Institute of Technology (MIT), Cambridge, MA, USA, in 1990.

He is currently a Professor with the Department of Civil and Environmental Engineering, MIT. He is also the Science Team Lead for the National Aeronautics and Space Administration's Soil Moisture Active and Passive mission that was launched on January 31, 2015. His research interests include terrestrial remote sensing, data assimilation, and coupled land–atmosphere systems modeling.

Dr. Entekhabi is a Fellow of the American Meteorological Society and the American Geophysical Union.

Joel T. Johnson (Fellow, IEEE) received the B.E.E. degree in electrical engineering from the Georgia Institute of Technology, Atlanta, GA, USA, in 1991, and the S.M. and Ph.D. degrees in electrical engineering and computer science from the Massachusetts Institute of Technology, Cambridge, MA, USA, in 1993 and 1996, respectively.

He is currently the Burn and Sue Lin Professor with the Department of Electrical and Computer Engineering and ElectroScience Laboratory, The Ohio State University, Columbus, OH, USA. His research interests include microwave remote sensing, propagation, and electromagnetic wave theory.

Dr. Johnson is a member of commissions B&F of the International Union of Radio Science (URSI), and a member of Tau Beta Pi, Eta Kappa Nu, and Phi Kappa Phi. He was the recipient of the 1993 Best Paper Award from the IEEE Geoscience and Remote Sensing Society, was named an Office of Naval Research Young Investigator, the National Science Foundation Career Award, and PECASE Award in 1997 and was recognized by the U.S. National Committee of URSI as a Booker Fellow in 2002.

Christopher A. Shuman received the B.A. (Hons.) degree with *cum laude* in geology from Moravian College, Bethlehem, PA, USA, in 1982, and the M.S. degree in geology and the Ph.D. degree in geoscience from the Pennsylvania State University, State College, PA, USA, in 1987 and 1992.

From 1992 to 1994, he held a postdoctoral appointment with the Earth System Science Center and the Department of Geosciences, Penn State. From 1994 to 1999, he held postdoctoral appointments with the National Research Council and the Universities Space Research Association, NASA's Goddard Space Flight Center. From 1999 to 2001, he was an Assistant Research Scientist with the Earth System Science Interdisciplinary Center, University of Maryland. From 2001 to 2007, he was a Physical Scientist with NASA's Goddard Space Flight Center and a Deputy Project Scientist for the ICESat Mission (2001–2005). He is currently an Associate Research Professor with the Baltimore County's Joint Center for Earth System Technology based at NASA's Goddard Space Flight Center's Cryospheric Sciences Laboratory, Institute for Research in Environmental Sciences, University of Maryland, College Park, MD, USA. He has contributed to research on *in situ*, satellite, and modeled temperature datasets from Greenland, and also changes to Antarctic ice shelves and major outlet glaciers. He has authored or coauthored research papers on ice elevation changes and glacier mass losses using altimetry in combination with other remote sensing in the Antarctica Peninsula, on the accuracy of the first ICESat mission's data over Antarctica's large subglacial lakes. He has also worked on composite temperature records derived from automatic weather stations, passive microwave data from SMMR and SSM/I, and IR data from satellite sensors. He has successfully matched those records through stratigraphic correlation with stable isotope temperature proxy profiles in shallow snow layers. He has worked extensively in Greenland (7 deployments) and Antarctica (6 field deployments plus multiple NASA Operation Ice Bridge flights from Punta Arenas, Chile). He began his cryospheric career helping to date the 3054-m-long Greenland Ice Sheet Project 2's (GISP2) deep ice core in 1992.

John S. Kimball received the B.A. and M.A. degrees in physical geography from San Diego State University, San Diego, CA, USA, in 1987 and 1990, respectively, and the Ph.D. degree in bioresource engineering from Oregon State University, Corvallis, OR, USA, in 1995.

He is currently a Professor of Systems Ecology and the Director of the Numerical Terradynamic Simulation Group, University of Montana, Missoula, MT, USA. He has contributed to more than 190 peer-reviewed scientific publications in his field.

Dr. Kimball was on several NASA mission teams, developing satellite environmental applications designed to meet NASA Earth Science objectives.

Zoe R. Courville photograph and biography not available at the time of publication.